 doi:10.20944/preprints202110.0240.v2

Article

Graphene prepared via the dry ice in flames method and its purification using different routes: a comparative study

Eduardo Cuadros-Lugo [1], Harby A. Martinez-Rodríguez [1,2], Daniel Lardizabal-Gutierrez [1], Ivanovich Estrada-Guel [1], Jose M. Herrera-Ramirez [1,*] and Caleb Carreño-Gallardo [1,*]

[1] Centro de Investigación en Materiales Avanzados, CIMAV, Miguel de Cervantes 120, Chihuahua, 31136 México; eduardo.cuadros@cimav.edu.mx (E.C.L.); harby.martinez@cimav.edu.mx (H.A.M.R.); daniel.lardizabal@cimav.edu.mx (D.L.G.); ivanovich.estrada@cimav.edu.mx (I.E.G.); martin.herrera@cimav.edu.mx (J.M.H.R.); caleb.carreno@cimav.edu.mx (C.C.G.)

[2] Grupo de propiedades térmicas dieléctricas de compósitos, Universidad Nacional de Colombia, sede Manizales, Colombia

* Correspondence: martin.herrera@cimav.edu.mx, Tel.: +52 614 439-48-27; caleb.carreno@cimav.edu.mx, Tel.: +52 614 439-48-16

Abstract: Although the dry ice method used to synthesize exfoliated graphite/graphene is little known and used, it has significant advantages over others: it is low cost, simple, and a large quantity of material can be obtained using some inorganic and highly available acids (which can be reused). Despite the above advantages, the main reason for its incipient development is the resulting presence of magnesium oxide in the final product. In the present work, three different treatments were tested to remove this remnant using some acid chemical leaching processes, making use of hydrochloric acid, aqua regia, and piranha solution. Based on the experimental evidence, it was found that using aqua regia and combining the leaching process with mechanical milling was the most efficient way of removing such a remnant, the residue being only 0.9 wt.%. This value is low when compared to that obtained with the other acid leaching solutions and purification process (2.8 - 29.6 wt.%). A mandatory high-energy mechanical milling stage was necessary during this treatment, in order to expose and dissolve the highly insoluble oxide without secondary chemical reactions on the graphenes. High-energy mechanical milling is an effective route to exfoliate graphite/graphene, which allows the magnesium oxide to be more susceptible to acid treatment. The obtained surface area was 504 m^2g^{-1}; this high value resulting from the intense exfoliation can potentiate the use of this material for a wide variety of applications.

Keywords: graphene; dry ice; mechanical milling; magnesium oxide

1. Introduction

Although 16 years have passed since its discovery, graphene is still of great interest to the scientific community [1]. Its applications cover multiple fields such as sensors, composite strengthening [2], hydrogen storage, and lithium-ion batteries, among others. The number of articles written on these topics since 2013 is around 15000 per year. Today, several synthesis methods are well known, being some of them the Hummer route [3], laser ablation, CVD [4], and high-energy milling [5]. Most of these methods involves serious disadvantages such as environmental pollution concerns [6] due mainly to the use of toxic reagents like sulfuric acid [7], potent reducing agents like hydrazine [8], or hazardous aromatic solvents like toluene, benzene, etc. [9]. Some others need expensive equipment for their production or require the use of high-purity gases [10]. The synthesis method using carbon dioxide as a precursor, which is known as dry ice in flames method, was developed by Chakrabarti and co-workers [11]. The method consists of igniting magnesium metal in a carbon dioxide (CO_2) atmosphere using a block of dry ice. This results

 doi:10.20944/preprints202110.0240.v2

in a highly exothermic reaction, reaching a temperature above 2500 °C, enough to perform the following chemical reaction [12]:

$$2\ Mg(s) + CO_2(g) \rightarrow 2MgO\ (s) + C\ (s)$$

The obtained products are magnesium oxide (MgO) and carbon (C) in graphite form. The latter can be presented in different forms, from exfoliated graphite to graphene. While exfoliated graphite can have large clusters of hundreds of graphene layers, graphene is made up of only a few sheets (~10). The main disadvantage of this method lies with the product separation: magnesium oxide from exfoliated graphite and graphenes [13]. The predominant purification method reported in different studies consists of a chemical dissolution with hydrochloric acid (HCl), forming magnesium chloride ($MgCl_2$), which is soluble in water, and its elimination by washing with demineralized water until a neutral pH is reached, then the purified exfoliated graphite is dried [13, 14]. Unfortunately, there is a problem related to a considerable amount of oxide (up to 5 at.%), which is impossible to remove, this remnant contamination being undesirable for some applications [15, 16]. Even though this production method has numerous advantages such as low production costs, in addition to the fact that the amount of obtained product is far above the reached through other synthesis techniques used [17]. Even when the process uses acid for purification, the washing waters are quickly neutralized, avoiding their corrosive nature. For all these reasons, some authors consider it an eco-friendly method [18, 19].

The present study proposes different chemical purification routes of the dry ice in flames products because magnesium oxide is not easy to dissolve fully. For this purpose, three acid solutions, namely hydrochloric acid, aqua regia, and piranha solution, were tested, combining the leaching process with high-energy ball milling at reduced processing times. To follow the changes and processing differences, some samples of the exfoliated graphite/graphene were analyzed before and after the purification process through different characterization techniques, such as Raman spectroscopy, surface area analysis (BET), transmission electron microscopy (TEM), and thermogravimetric analysis (TGA).

2. Materials and Methods

2.1. Synthesis Method

The exfoliated graphene-graphite synthesis was carried out using a 20-cm solid cubic block of dry ice (solid carbon dioxide), to which a cavity of 10 cm in deep and 7 cm in diameter was made. 20 g of pure magnesium chips (Sigma-Aldrich, 6-35 mesh, 99.98% purity) were introduced in the cavity and the reaction was induced through a spark provided by a butane gas lighter (Figure 1). This operation was repeated until a total of 150 g was obtained; as mentioned, the obtained material consisted of a mixture of graphite/graphene and magnesium oxide in powder form.

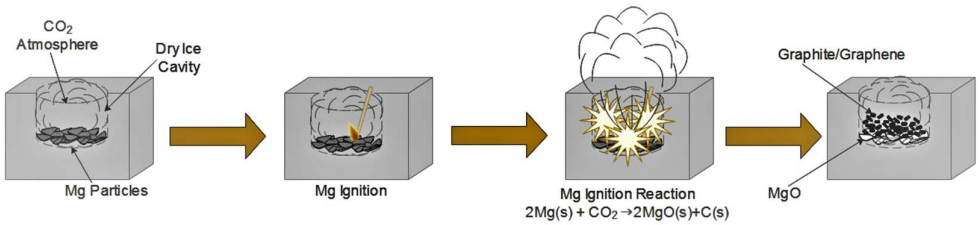

Figure 1. Descriptive diagram of the synthesis route to obtain exfoliated graphite/graphene.

2.2. Purification Methods

The obtained powders were subjected to a chemical purification process based on three different acid solutions (Table 1).

 doi:10.20944/preprints202110.0240.v2

Table 1. Acid leaching solutions used during the purification processing.

Name	Composition	Nomenclature
Hydrochloric acid	HCl 1M	LM1
Aqua regia	HNO_3:HCl 3:1 (in vol.)	LM2
Piranha solution	H_2SO_4:H_2O_2 (30 vol.%) 3:1	LM3

A general scheme of the involved processes used to remove magnesium oxide is presented in Figure 2. Two purification processes were performed in the present research. The first process (PP1) consisted of leaching the graphite/graphene synthesis product with the three solutions indicated in Table 1, followed by vacuum filtering. In the second process (PP2), the material obtained from PP1 was further processed by mechanical milling. Then it was leached again with the same acid solution of the first leaching process and vacuum filtered. The obtained samples were characterized through the techniques mentioned above. The main reason to complement the leaching with high-energy ball milling is that the mechanical milling causes the removal of the carbon layers that are firmly attached to the MgO and, as a consequence, it promotes an increased chemical attack which enhances the dissolution of these unwanted particles. Also, the high-energy mechanical milling helps to promote the exfoliation of the graphite from unexfoliated graphite [20].

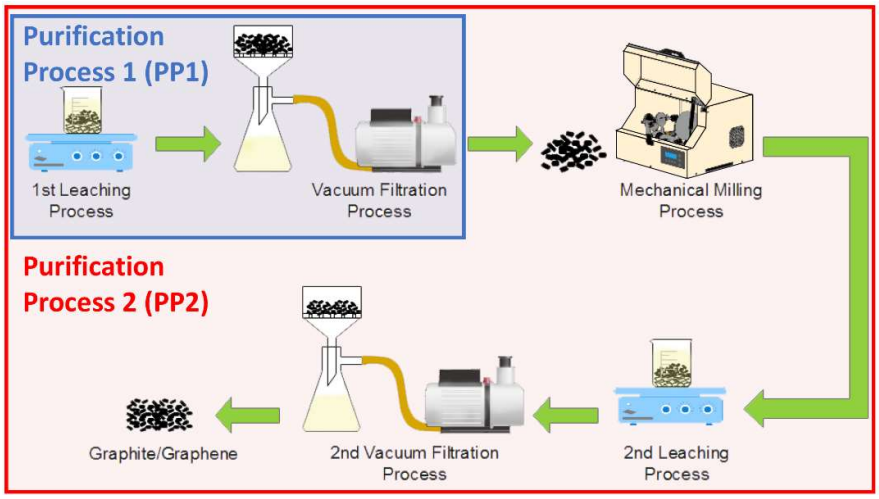

Figure 2. Illustrative diagram of sample purification processing.

2.3 *Leaching*

The leaching process was set to 24 h for all samples under a constant stirring at 80 °C [21].

2.4 *Vacuum Filtering*

After the leaching process, a vacuum filtration process was carried out in the wet mixtures using a 500-mL Kitasato flask coupled with a Büchner funnel and a Whatman filter paper number 42. The powders were washed with demineralized water until reaching neutral pH and dried in a laboratory stove at 100 °C overnight.

2.5 *Milling*

High-energy milling was carried out using a Spex 8000M device, processing 1 g of the washed and dried sample with a milling time of 30 min. A hardened steel vial and 13-mm balls were used; the ball-to-powder weight ratio was kept at 30:1 (in weight) for all experimental runs and no process control agent was added during the milling.

 doi:10.20944/preprints202110.0240.v2

2.6. *Characterization Techniques*

The presence of phases and their crystalline characteristics were studied by X-ray diffraction (XRD) in a Panalytical X'Pert-Pro diffractometer working at 40 kV and 35 mA using Cu-Kα radiation with a wavelength of 0.154056 nm; the data were collected in the 2θ range from 5 to 80° with a step size of 0.2° per second. Thermogravimetric analysis (TGA) was performed using a TA Instrument model Q600, with a heating ramp of 10 °C/min from room temperature to 800 °C under an airflow of 50 cm^3/min. Raman spectrometry was performed using a LabRam HR VIS-633 microscope developed by Horiba equipped with a He-Ne laser source. Transmission electron microscopy (TEM) using a Hitachi 7700 microscope and high-resolution transmission electron microscopy (HRTEM) using a TEM JEOL JEM 2200FS microscope were employed to analyze the synthesized graphenes. N_2 adsorption-desorption isotherms were obtained by the Brunauer-Emmett-Teller (BET) method in a Quanta chrome model Nova 4200e analyzer, taking 11 points of 0.05 to 0.3 of relative pressure (P/P_0); from this analysis the surface area and the pore distribution were determined. X-ray photoelectron spectroscopy (XPS) spectra were collected on a Thermo Scientific model Escalab 250Xi spectrometer equipped with a monochromator, which was used to identify the chemical bonding in the C 1s region.

3. Results

3.1. *Characterization of Graphene Powders*

TEM studies were carried out to determine the phase coexistence, particle size, morphology and microstructure of samples. The obtained material from the dry ice synthesis process without any additional processing was analyzed. Figure 3 shows a TEM micrograph where a mixture of graphite/graphene structures is observed, as well as the presence of a considerable concentration of MgO in the form of cubical particles. The proposed purification processing methods are intended to remove these agglomerated and exposed particles.

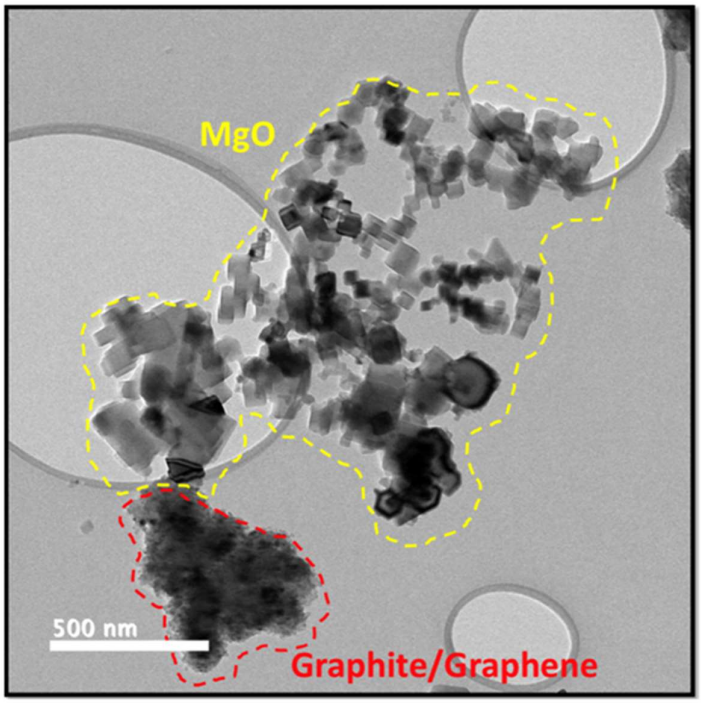

Figure 3. TEM image of raw sample obtained after the synthesis.

 doi:10.20944/preprints202110.0240.v2

Figure 4 shows HRTEM micrographs of samples after the purification processes. Micrographs in Figures 4a-c correspond to samples processed by the first purification process (PP1), where the presence of graphene sheets and embedded MgO nanoparticles is clear. These nanoparticles have the characteristic cubic geometry, whose size dispersion varies from 10 to 20 nm. Micrographs in Figures 4d-f correspond to samples subjected to the first purification process (PP1) followed by mechanical milling and a second purification process (PP2) to remove as much as possible the MgO phase. These images show clear evidence of a graphene sheet (Figure 4d), where the van der Waals interlayer attractions allowed the nanosheets to slide each other perpendicularly to the c-axis. Still, enough attraction prevents the complete formation of individual graphene monolayers; the diffraction contrast is related to thickness variation, denoting the presence of multiple graphene layers and polycrystalline structures with randomly oriented grains. After the second leaching process, the relative concentration of MgO particles decreased considerably compared to samples from the first leaching process.

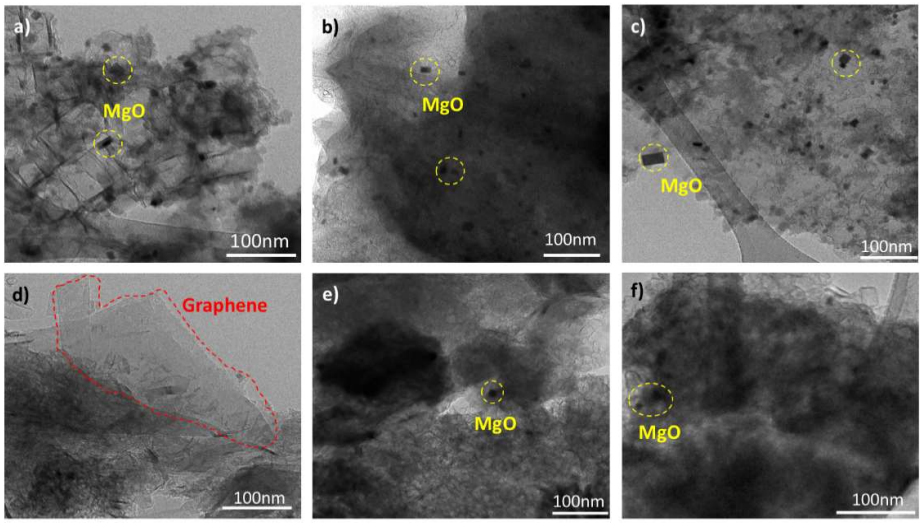

Figure 4. HRTEM images of a) LM1-PP1, b) LM2-PP1, c) LM3-PP1, d) LM1-PP2, e) LM2-PP2, and f) LM3-PP2 samples.

Comparative X-ray diffraction patterns of samples under different processing conditions are seen in Figure 5. Figure 5a presents the diffractograms of samples after the first purification process. The indexed diffraction peaks located at $2\theta \approx 26$ and 54° are attributed to the planes (002) and (004), respectively, both corresponding to a turbostratic structure (JCPDS 41-1487). The signals at 37, 43, 63, 75 and 78° are correlated with the planes (111), (200), (220), (311), and (222), respectively, and are attributed to magnesium oxide (JCPDS 78-0430). Figure 5b presents the diffractograms of samples after the second purification process; although the MgO is still present, a significant decrease in its signals is evidenced. Likewise, graphene oxide was observed and identified at $2\theta \approx 12.3°$ in the LM1-PP2 sample [21]. Due to the instrumental restriction of XRD, this analysis does not allow us to differentiate which purification method is better quantitatively.

Preprints (www.preprints.org) | NOT PEER-REVIEWED | Posted: 13 January 2022 doi:10.20944/preprints202110.0240.v2

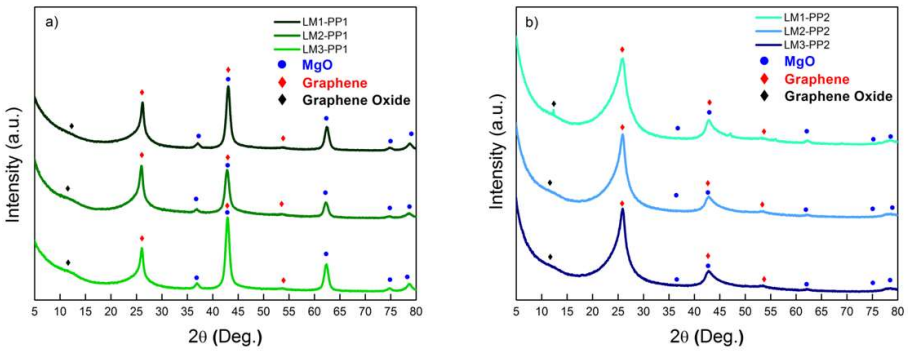

Figure 5. XRD patterns of a) PP1 and b) PP2 samples.

The number of layers along the c-axis (N_c) of graphene samples was calculated by the equation described by Seehra et al. [22] (Equation 1), where L_c is the apparent crystallite size, which was determined from the Scherrer equation (Equation 2) and d_{002} is the interplanar spacing of for the (002) plane, which was calculated from the Bragg's Law (Equation 3) [23, 24].

$$Nc = \frac{L_c}{d_{002}} \quad (1)$$

$$L_c = \frac{k\lambda}{\beta cos\theta} \quad (2)$$

$$d_{002} = \frac{n\lambda}{2sin\theta} \quad (3)$$

As shown in Table 2, the number of layers decreases after going through the purification process 2.

Table 2. Numbers of layers in graphene samples.

Sample	Number of layers
LM1-PP1	32
LM2-PP1	26
LM3-PP1	31
LM1-PP2	23
LM2-PP2	13
LM3-PP2	26

Figure 6 displays the results of Raman spectroscopy. The Raman spectra evidence that all samples are basically composed of a carbonaceous matrix with representative signals related to graphitic structures; these signals are commonly described as D, G, and 2D bands, which were detected at 1350, 1580, and 2600 cm^{-1}, respectively [25]. As it is well known, the D band is related to lattice disorder and sp3 defects in graphenes, while the G band is the result of in-plane C-C symmetric stretching vibrations and is associated with the sp2 structure of carbon [26]. The 2D band is correlated with the overtone of the D band [27]. The D-band and G-band (I_D/I_G) intensity ratio is used to evaluate the degree of disorder and defects in the graphitic structure. As can be observed, the I_D/I_G ratio was affected by the mechanical milling process increasing from 0.91 (average of the three leaching processes) for the first purification process (PP1) to 1.24 for the second purification process (PP2), which involves mechanical milling, leading to a yield of 99% from the PP2. The intensity of the D band at 1322 cm^{-1} of samples purified through the PP2 process is greater than that of PP1 samples. This increment in intensity evidences that defects increased due to the mechanical milling process. Consequently, an increase in

 doi:10.20944/preprints202110.0240.v2

destructive exfoliation was produced and correlated with the broadening and decreasing in intensity observed in the X-ray patterns (Figure 5).

The intensity of the 2D bands is lower for the PP2 samples than PP1, which can be attributed to defects in the graphene structure [28-30]. This decrease in intensity is characteristic to the disorder in the c-axis [31, 32] and turbostratic structure formation derived from the disordered graphene layer arrangement resulting from the chemical reaction [12]. Also, the 2D band is inextricably linked to the electronic band structure of graphene and is a good indicator of a more graphene-like structure; this can be confirmed with the XPS results by the presence of the sp2 bonds, as will be seen below [33]. According to the previous references, the appearance of this band is related to defects or doping in the graphitic structure.

A Raman analysis of MgO was performed to discard the contribution of its bands. The MgO spectrum is dominated by two main bands of approximately the same intensity, located at 1500 and 1935 cm^{-1} [34]. As shown in Figure 7, the 1500 cm^{-1} MgO band could overlap with the G-band of graphene. However, comparing the MgO spectrum with those of processed samples (inset in Figure 7), the presence of the 1935 cm^{-1} MgO band is not observed. Based on these findings, it can be assumed that there is no contribution of MgO bands in the analyzed samples. Therefore, it can be expected that the result of the I_D/I_G ratio calculation is not affected. The split shape in the G-band can be seen in all the samples and is attributed to the D' band located at ~1610 cm^{-1}. The appearance of the D' band is caused by defects in the carbon structure in all the analyzed samples [35, 36].

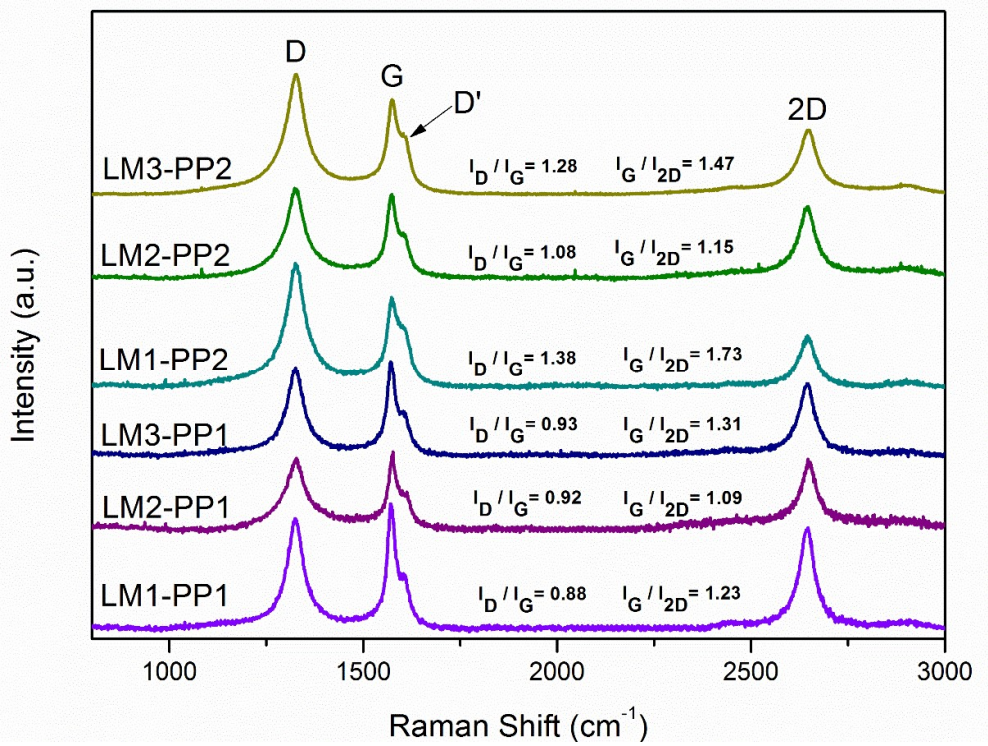

Figure 6. Comparative Raman spectra of PP1 and PP2 leached samples.

 doi:10.20944/preprints202110.0240.v2

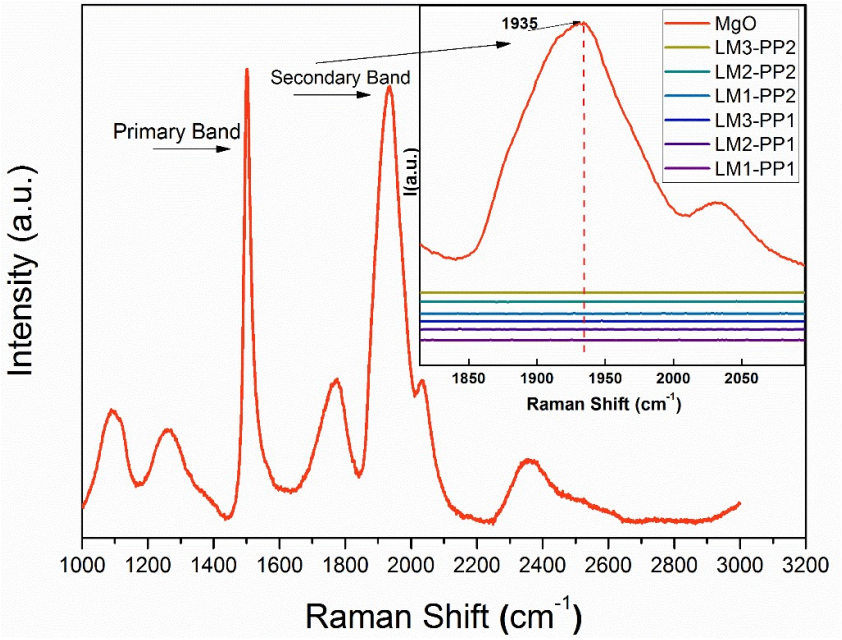

Figure 7. Comparative Raman spectra of MgO and leached samples.

Figure 8 presents the results of the BET analysis. The isotherms of both the PP1 and PP2 samples show a Type IV (mesoporous) structure, according to the BDDT classification. The amount of adsorption is less in the low-pressure area, increasing sharply in the high-pressure area. Likewise, the PP1 and the PP2 solid solutions present a Type B hysteresis loop, according to the Boer definition, showing the same behavior in all the samples. This phenomenon is related to graphene materials, where the pores correspond to the spaces between the graphite sheets. A wide pore distribution was calculated (60 – 180 Å in diameter), which is related to a heterogeneous pore diameter of the materials [37]. One of the main effects of the solid adsorbent materials is presented in the interface, which generates the adsorption [38].

Table 3 presents the results of the surface area (SA) analysis attained through the BET method. The values for PP1 samples are in the range of 300-390 m^2g^{-1}, while the PP2 samples presented higher and uniform values in the range of 500-505 m^2g^{-1}. With this, it can be pointed out that SA is a dependent variable closely related to the purification treatment.

Preprints (www.preprints.org) | NOT PEER-REVIEWED | Posted: 13 January 2022 doi:10.20944/preprints202110.0240.v2

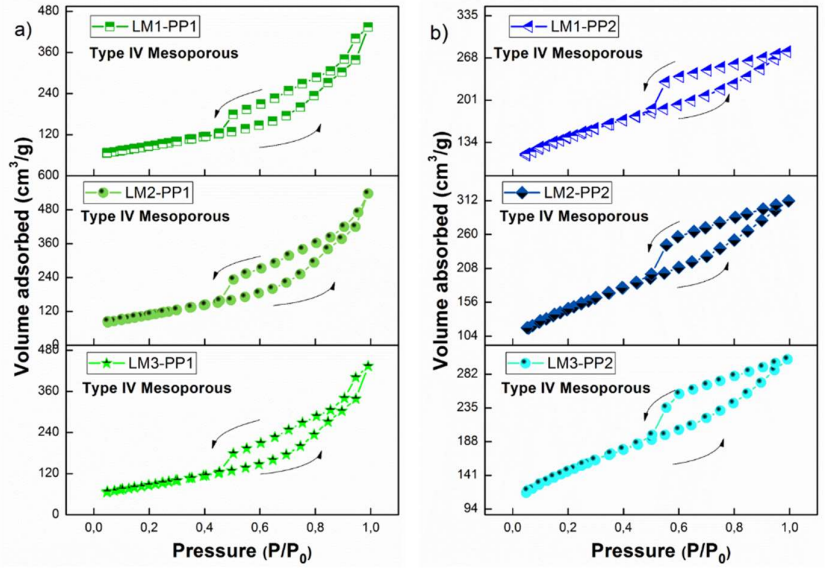

Figure 8. BET N_2 adsorption-desorption isotherms and hysteresis loop: a) PP1 and b) PP2 samples.

Table 3. Summary chart of SA (in m^2g^{-1}) of samples after leaching.

Sample	Surface Area
LM1-PP1	332.6 ± 1
LM2-PP1	389.0 ± 1
LM3-PP1	312.6 ± 1
LM1-PP2	504.8 ± 1
LM2-PP2	503.4 ± 1
LM3-PP2	502.0 ± 1

X-ray photoelectron spectroscopy was performed to characterize the graphene sheets and the oxygenated functional groups present in the samples after the leaching steps. As an example, Figure 9 shows the XPS spectra for samples leached with aqua regia with both purification process (LM2-PP1 and LM2-PP2). After deconvolution, a highly intense peak corresponding to the sp2 band at 284.4 eV was found, which are assignable to graphene [21]. Further, in a lesser extent, the C-C band (285.0 eV) assignable to sp3 hybridizion carbon and the C-O band (286.2 eV) assignable to graphene oxide were obtained. In the case of sample leached with hydrochloric acid with the purification process 1 (LM1-PP1) the peak of the C=O band was found at 290.2 eV. The presence of oxidized groups is related to the different acid treatments; it is worth mentioning that the dry ice in flames method produces graphenes that do not start from oxidized graphite (GO) reduction processes as other synthesis methods do. The area percentage corresponding to each type of bond was determined and the results are summarized in Table 4. A chemical reduction is observed in all the samples of the oxidized groups after the second treatment (PP2), which present an average of ~12%, compared with ~21% for samples after the first treatment (PP1).

Preprints (www.preprints.org) | NOT PEER-REVIEWED | Posted: 13 January 2022 doi:10.20944/preprints202110.0240.v2

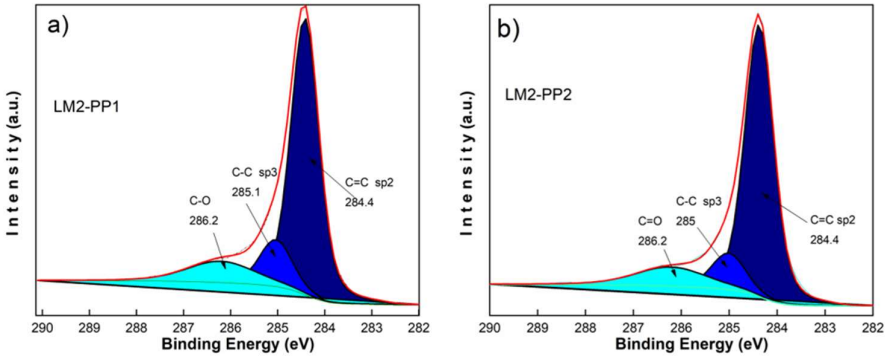

Figure 9. Comparative XPS analysis of PP1 and PP2 processing of LM2 samples.

Table 4. Area percentages of the C 1s XPS spectra for the different treatments.

Binding	LM1-PP1	LM1-PP2	LM2-PP1	LM2-PP2	LM3-PP1	LM3-PP2
sp2	50 %	70 %	72 %	75 %	74 %	79 %
sp3	15 %	15 %	14 %	12 %	12 %	10 %
C-O	26 %	15 %	14 %	13 %	14 %	11 %
C=O	9 %	----	----	----	----	----

The thermogravimetric analysis (TGA) curves show the mass loss of samples as a function of the temperature (Figure 10). The mass loss related to carbon oxidation occurs in the range of 500 to 750 °C, leaving a solid residue mainly composed of magnesium oxide. The final residue percentage of PP1 samples is between 22.8 and 29.6%, which is correlated as MgO (Figure 10a). This large amount of residue is the main reason why this synthesis method has not been widely developed. For PP2 samples (Figure 10b), the final residue percentage ranges from 0.9 to 2.9%, standing out the leaching process where aqua regia is used (LM2) with a residue of only 0.9%. TGA analysis is a fundamental tool to quantitatively evaluate the best purification treatment (related to residue generation after calcination) [39].

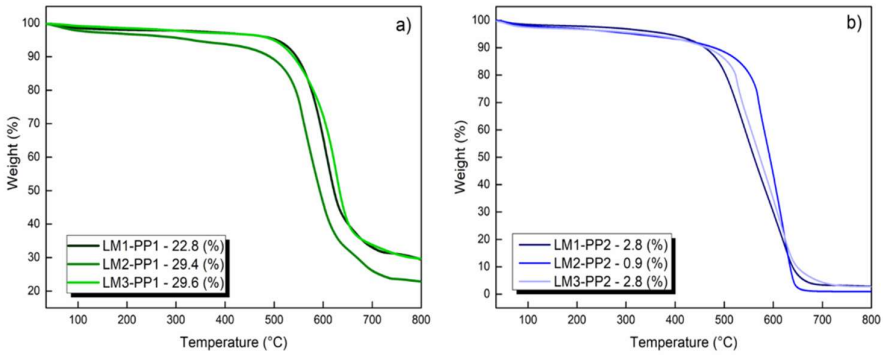

Figure 10. Comparative thermograms and residues of leached samples a) PP1 and b) PP2.

4. Discussion

 doi:10.20944/preprints202110.0240.v2

Based on the evidence obtained by TEM, a mechanism for the high concentration of unreacted MgO during the dry ice in flames synthesis method is proposed, which is schematized in Figure 11. Figure 11a shows a general view of the MgO nanoparticles surrounded by graphite. The TEM image in Figure 11b evidences that the MgO nanoparticles are covered with several graphene layers, preventing physical contact with the leaching chemical from achieving their complete dissolution. These layers may be present in different thicknesses spanning a few layers; if the material reaches many layers, it can induce graphite formation.

The XRD signal detected at $2\theta \approx 12.3°$ for the LM1-PP2 sample (Figure 5b) corresponds to the main diffraction peak of graphene oxide, which indicates a slight oxidation of graphene [21]. Such an oxidation could also have been generated in the other samples, but the signal is not appreciable in their diffractograms. It is said that the XRD resolution is between 0.5 and 1.0%, depending on the nature of the analyzed material. Thus, if the graphene oxide generated in our samples is below this resolution limit, it will not be possible to detect it by XRD.

The sp2-type carbon materials exhibit a Raman spectrum with a strong peak in the 2500 to 2800 cm^{-1} range, corresponding to the 2D band. This is a second-order two-phonon process, which strongly depends on the used frequency of the laser energy excitation [40]. The 2D band can be used to determine the number of graphene layers. This is mainly applied to graphene-multilayer-type structures, where the shape of the 2D band is quite different from that of single-layer graphene with more intense and sharper bands. In our case (Figure 12), the 2D band does not present significant differences neither in the peak shape nor in the shift value between PP1 and PP2 wash process, which was less than 3 cm^{-1}. In addition, no shoulders or overlaps or the presence of 2D1 and 2D2 bands are observed. However, the I_G/I_{2D} ratio has a contradictory behavior to the theoretical one. This behavior could be related to the synthesized material since it does not come from natural crystalline graphite, as most studies do. It is necessary to carry out future work to verify this behavior. We can say that the material is exfoliated as the high surface area results showed, as reported in Table 3.

It is worth mentioning that van der Waals forces play an important role, as they are responsible for linking these graphene sheets together during the graphite formation. Based on the surface area results, it can be assumed that most of the particles remain as exfoliated graphite consisting of a few hundred graphene layers. Note that the theoretical surface area value for graphene is 2700 m^2g^{-1} [41], which is well above the values found for the materials synthesized in this investigation; this may indicate how far we are from generating a graphene monolayer. The mechanical milling process promotes the graphite exfoliation and induces an increase of surface exposure of the oxide; this facilitates the acid attack and the subsequent dissolution process (Figure 11c).

Another clear advantage of this purification process is related to the processing time to obtain a relatively elevated surface area (~500 m^2g^{-1}). Indeed, such a value of the surface area is achieved after 16 h when using high-energy ball milling obtained from natural graphite [20, 42, 43]. In contrast, the time used to carry out the exfoliation in this work was only 30 min, which is reflected in a considerable saving of time and is able to process a greater quantity of material. Furthermore, our SA value is almost twice compared to synthesis methods like the reduction of graphene oxide, where a surface area of 298.2 m^2g^{-1} was obtained [44].

Preprints (www.preprints.org) | NOT PEER-REVIEWED | Posted: 13 January 2022 doi:10.20944/preprints202110.0240.v2

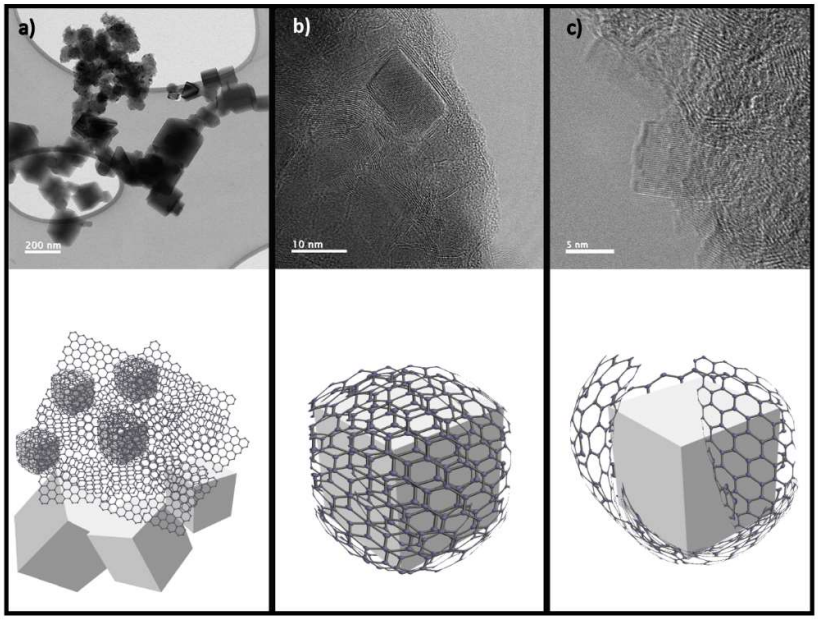

Figure 11. TEM micrographs and proposed dissolution mechanism.

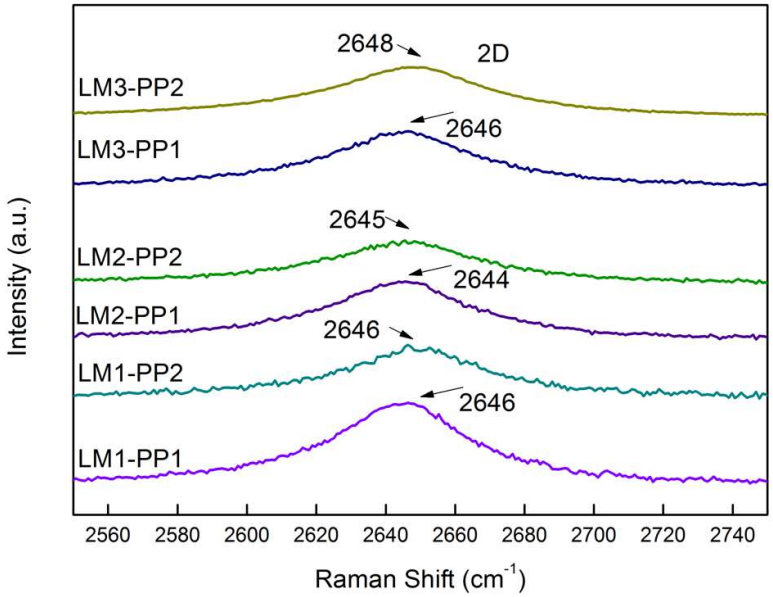

Figure 12. 2D band comparison of the processes PP1 and PP2.

5. Conclusions

The dry ice in flames method was successfully used for exfoliating graphite/graphene. This method can be a potential alternative to perform this process due to its low cost, simplicity and high scalability. The proposed mechanical milling stage and a second leaching process (PP2) are essential for the effective removal of MgO. Based on the experimental results, the treatment using aqua regia in the PP2 process (LM2-PP2) was the most effective, reaching a value of 0.9 wt.% of MgO residues. This route is more effective than

that of the treatment with hydrochloric acid (LM1), which is universally used on this subject. The study opens the doors for using the purified exfoliated graphite for various applications where a high surface area is necessary, such as in catalysis and removal of solvents and heavy metals. Through the surface area analysis, it is concluded that mechanical milling helps to increase the surface area in the analyzed samples, thus giving way to obtaining a graphene of greater purity.

Author Contributions: Conceptualization, C.C.G. and J.M.H.R.; methodology, C.C.G., I.E.G., D.L.G; formal analysis, E.C.L., H.A.M.R., I.E.G., D.L.G., C.C.G. and J.M.H.R.; investigation, E.C.L., H.A.M.R., I.E.G., D.L.G., C.C.G. and J.M.H.R.; writing—original draft preparation, C.C.G. and J.M.H.R.; writing—review and editing, I.E.G., D.L.G., C.C.G. and J.M.H.R; visualization, E.C.L. and H.A.M.R.; supervision, I.E.G., C.C.G. and J.M.H.R.; project administration, C.C.G. and J.M.H.R. All authors have read and agreed to the published version of the manuscript.

Funding: This research received no external funding.

Acknowledgments: The authors would like to thank the valuable technical assistance of R. Ochoa Gamboa, P. Pizá Ruiz, L. de la Torre Saenz, J.E. Ledezma Sillas and E. Guerrero Lestarjette.

Conflicts of Interest: The authors declare that they have no known competing financial interest or personal relationships that could have influenced the work reported in this paper.

References

1. Novoselov, K.S., et al., *A roadmap for graphene.* Nature, 2012. **490**(7419): p. 192-200.
2. Rashad, M., et al., *Effect of Graphene Nanoplatelets addition on mechanical properties of pure aluminum using a semi-powder method.* Progress in Natural Science: Materials International, 2014. **24**(2): p. 101-108.
3. Paulchamy, B., G. Arthi, and L. Bd, *A Simple Approach to Stepwise Synthesis of Graphene OxideNanomaterial.* Journal of Nanomedicine & Nanotechnology, 2015. **6 (1)**: p. 1000253.
4. Castro Beltrán, A., et al., *Obtención de grafeno mediante la reducción química del óxido de grafito.* Ingenierías, 2011. **14**(52): p. 34-42.
5. Kim, D., et al., *Synthesis of reduced graphene oxide/aluminum nanocomposites via chemical-mechanical processes.* Journal of Composite Materials, 2018. **52**(22): p. 3015-3025.
6. Luo, D., et al., *An improved method to synthesize nanoscale graphene oxide using much less acid.* Materials Today Physics, 2019. **9**: p. 100097.
7. Papageorgiou, D.G., I.A. Kinloch, and R.J. Young, *Mechanical properties of graphene and graphene-based nanocomposites.* Progress in Materials Science, 2017. **90**: p. 75-127.
8. Kairi, M.I., et al., *Toward high production of graphene flakes – a review on recent developments in their synthesis methods and scalability.* Journal of Materials Chemistry A, 2018. **6**(31): p. 15010-15026.
9. Jeon, I.Y., et al., *Edge-carboxylated graphene nanosheets via ball milling.* Proceedings of National Academic of Sciences U S A, 2012. **109**(15): p. 5588-93.
10. García Martínez, V., *Estudio de la estabilidad del óxido de grafeno con el tiempo*. 2013, Universidad de Oviedo.
11. Chakrabarti, A., et al., *Conversion of carbon dioxide to few-layer graphene.* Journal of Materials Chemistry, 2011. **21**(26): p. 9491-9493.
12. Zhang, J., et al., *Synthesis of graphene from dry ice in flames and its application in supercapacitors.* Chemical Physics Letters, 2014. **591**: p. 78-81.
13. Arifutzzaman, A., et al. *Fabrication and Characterization of graphene from solid carbon dioxide*. in *Advanced Materials Research*. 2015. Trans Tech Publ.
14. Shams, S.S., R. Zhang, and J. Zhu, *Graphene synthesis: a Review.* Materials Science-Poland, 2016. **33**(3): p. 566-578.

15. *Case Western Reserve University. (2012, March 26). Simple, cheap way to mass-produce graphene nanosheets. ScienceDaily. Retrieved November 8, 2021 from www.sciencedaily.com/releases/2012/03/120326160823.htm*. 2012.
16. Chakrabarti, A. and N.S. Hosmane, *Crystalline graphene and method of making crystalline graphene*. 2016: US.
17. Kim, T.H., et al., *Bulk synthesis of graphene-like materials possessing turbostratic graphite and graphene nanodomains via combustion of magnesium in carbon dioxide.* Carbon, 2019. **149**: p. 582-586.
18. Romero, A., et al., *Comparative study of different scalable routes to synthesize graphene oxide and reduced graphene oxide.* Materials Chemistry and Physics, 2018. **203**: p. 284-292.
19. Zaaba, N., et al., *Synthesis of graphene oxide using modified hummers method: solvent influence.* Procedia engineering, 2017. **184**: p. 469-477.
20. Mendoza-Duarte, J.M., et al., *Exfoliated Graphite Preparation based on an Eco-Friendly mechanochemical Route.* Journal of Environmental Chemical Engineering, 2020. **8**: p. 104370.
21. Tuz Johra, F., J. Lee, and W.-G. Jung, *Facile and safe graphene preparation on solution based platform.* Journal of Industrial and Engineering Chemistry, 2014. **20**: p. 2883–2887.
22. Albetran, H.M., *Structural Characterization of Graphite Nanoplatelets Synthesized from Graphite Flakes*. 2020.
23. Low, I.-M., H.M. Albetran, and M. Degiorgio, *Structural characterization of commercial graphite and graphene materials.* Journal of Nanotechnology and Nanomaterials, 2020. **1**(1): p. 23-30.
24. Low, I.M., et al., *A comparative study on crystallization behavior, phase stability, and binding energy in pure and Cr-doped TiO2 nanotubes.* Journal of Materials Research, 2013. **28**(3): p. 304-312.
25. Al-Sherbini, A.-S., et al., *Exfoliation of graphene sheets via high energy wet milling of graphite in 2-ethylhexanol and kerosene.* Journal of Advanced Research, 2017. **8**(3): p. 209-215.
26. Zhou, W., et al., *Creation of individual few-layer graphene incorporated in an aluminum matrix.* Composites Part A: Applied Science and Manufacturing, 2018. **112**: p. 168-177.
27. Zan, Y.N., et al., *Introducing graphene (reduced graphene oxide) into Al matrix composites for enhanced high-temperature strength.* Composites Part B: Engineering, 2020. **195**: p. 108095.
28. Caicedo, F.M.C., et al., *Synthesis of graphene oxide from graphite by ball milling.* Diamond and Related Materials, 2020. **109**: p. 108064.
29. Chen, C.-N., Y.-L. Chen, and W.J. Tseng, *Surfactant-assisted de-agglomeration of graphite nanoparticles by wet ball mixing.* Journal of materials processing technology, 2007. **190**(1-3): p. 61-64.
30. Lin, F., et al., *Synergistic effects of TiC and graphene on the microstructure and tribological properties of Al2024 matrix composites.* Advanced Powder Technology, 2021. **32**(10): p. 3635-3649.
31. Ferrari, A.C. and J. Robertson, *Resonant Raman spectroscopy of disordered, amorphous, and diamondlike carbon.* Physical review B, 2001. **64**(7): p. 075414.
32. *Walther*. [July 15, 2021]; Available from: https://carl-walther.de/.
33. Arul, R., et al., *The mechanism of direct laser writing of graphene features into graphene oxide films involves photoreduction and thermally assisted structural rearrangement.* Carbon, 2016. **99**: p. 423-431.
34. Weibel, A., et al., *Fast and easy preparation of few-layered-graphene/magnesia powders for strong, hard and electrically conducting composites.* Carbon, 2018. **136**: p. 270-279.
35. Shao, Y., et al., *Highly durable graphene nanoplatelets supported Pt nanocatalysts for oxygen reduction.* Journal of Power Sources, 2010. **195**(15): p. 4600-4605.
36. Mallineni, S.S.K., et al., *Influence of dopants on the impermeability of graphene.* Nanoscale, 2017. **9**(18): p. 6145-6150.
37. Iakunkov, A. and A.V. Talyzin, *Swelling properties of graphite oxides and graphene oxide multilayered materials.* Nanoscale, 2020. **12**(41): p. 21060-21093.

38. Qiu, T., et al., *The preparation of synthetic graphite materials with hierarchical pores from lignite by one-step impregnation and their characterization as dye absorbents.* RSC Advances, 2019. **9**(22): p. 12737-12746.
39. Park, J., et al., *Properties of Graphene/Shape Memory Thermoplastic Polyurethane Composites Actuating by Various Methods.* Materials, 2014. **7**.
40. Raja, P.M.V. and A.R. Barron, *Characterization of Graphene by Raman Spectroscopy.*
41. Priyanka, V., et al., *Physicochemical exfoliation of graphene sheets using graphitic carbon nitride.* New Journal of Chemistry, 2019. **43**(41): p. 16200-16206.
42. Mahmoud, A.E.D., A. Stolle, and M. Stelter, *Sustainable Synthesis of High-Surface-Area Graphite Oxide via Dry Ball Milling.* ACS Sustainable Chemistry & Engineering, 2018. **6**(5): p. 6358-6369.
43. Dash, P., et al., *Preparation of graphene oxide by dry planetary ball milling process from natural graphite.* RSC Advances, 2016. **6**(15): p. 12657-12668.
44. Tiwari, J.N., et al., *Reduced graphene oxide-based hydrogels for the efficient capture of dye pollutants from aqueous solutions.* Carbon, 2013. **56**: p. 173-182.